JOURNAL OF AIRCRAFT
Vol. 34, No. 3, May–June 1997

Analytic Sensitivities and Approximations in Supersonic and Subsonic Wing/Control Surface Unsteady Aerodynamics

Wei-Lin Li* and Eli Livne†
University of Washington, Seattle, Washington 98195

Development of efficient, design-oriented analysis techniques and associated approximations for wing/control surface unsteady aerodynamics is crucial to the success of any multidisciplinary aeroservoelastic optimization of airplanes including active control technology. A design-oriented capability for unsteady supersonic aerodynamics for planar wing/control surface configurations is presented here. Explicit expressions for aerodynamic influence coefficients make it possible to efficiently obtain analytic sensitivities of generalized aerodynamic loads with respect to planform shape. Examination of the mathematical structure of the discretization used, similar to other aerodynamic panel methods, reveals sources of discontinuity of derivatives with respect to shape in the supersonic case. Sources of nonsmooth behavior of the unsteady aerodynamic loads in subsonic flow are identified and eliminated. The accuracy and computational cost of alternative approximation techniques are studied. A second-order approximation technique based on the direct and adjoint solutions at a reference configuration is presented. Experience and insight are gained in the area of design-oriented and approximate unsteady aerodynamics, to be used in the nonlinear programming/approximation concepts approach to engineering optimization.

Nomenclature

$[A(k, M_\infty)]$	= matrix of aerodynamic influence coefficients
b	= reference length
DV	= planform shape design variable
d_k	= half-width of kth aerodynamic element
$\{f\}$	= approximate aerodynamic force vector
$\{f\}_k$	= vector of forces on elements caused by the motion in mode k
$\{H_k\}$, $\{\partial H_k/\partial x\}$	= displacement vectors and the slopes for the downwash points because of motion in the kth generalized displacement
$\{h_k\}$, $\{\partial h_k/\partial x\}$	= vectors of displacements and slopes of deformation because of motion in mode k
i	= $\sqrt{-1}$ (unit pure imaginary number)
K	= kernel function of the lifting surface integral equation
$\bar{K}$	= unsteady factor
K_0	= steady part of the kernel
$\hat{k}$	= reduced frequency
M_∞	= flight Mach number
N	= number of aerodynamic boxes
$[Q]$	= generalized unsteady aerodynamic forces
Q_R, Q_I	= real and imaginary parts of the generalized aerodynamic force matrix
q_D	= dynamic pressure
U	= mainstream airspeed
X_1, X_2	= limits of integration, Eq. (2)
x_i, y_i	= coordinates of the ith downwash point
$\bar{x}_i$, $\bar{y}_i$	= coordinates of the ith unsteady factor evaluating point
x_0, y_0	= relative distance of sending point from receiving point
β	= $\sqrt{1 - M^2}$ in subsonic flow, and $\sqrt{M^2 - 1}$ in supersonic flow
$\{\eta\}$	= adjoint (reverse flow) solution
$\{\bar{\eta}\}$	= approximate adjoint solution
σ_k	= area of trapezoidal element k

Subscripts

p_i, q_i	= powers of x and y, respectively, for the ith polynomial term in a mode shape polynomial

Superscripts

T	= transpose
*	= adjoint (transpose, complex conjugate)

Received May 13, 1995; revision received Feb. 6, 1997; accepted for publication Feb. 17, 1997.

*Research Associate, Department of Aeronautics and Astronautics. Member AIAA.

†Associate Professor, Department of Aeronautics and Astronautics. Associate Fellow AIAA.

Introduction

THE rapid progress in airplane multidisciplinary design optimization (MDO),[1] following the success of structural synthesis,[2–4] calls for more multidisciplinary interactions to be addressed as early as possible in the airplane design optimization process. Active control technology,[5–7] through its effects on aeroservoelastic stability, dynamic stresses caused by gusts, handling qualities, and passenger comfort, is an area of major importance. However, only a limited amount of experience has been gained to date in truly integrated aeroservoelastic synthesis.

The key to the success and practicality of realistic airplane configuration optimization involving aeroservoelastic constraints has been (as in the case of structural synthesis) the nonlinear programming and approximation concepts (NLP/AC) approach to engineering optimization.[8–10] Because of the high computational cost of each analysis in the interacting disciplines any effort to connect optimization algorithms directly to detailed analyses in each of the disciplines will lead to impractical computational times, since many function evaluations are required in the course of any realistic design optimization process. In NLP/AC, optimization is carried out using approximate, computationally fast, analysis techniques. Detailed analysis is used only to generate these approximations and fine-tune them. It is, thus, important to have efficient approximate analysis techniques in each of the disciplines involved. The

better the accuracy of an approximation technique, the wider the move limits that are used can be, the faster the convergence of the process is, and the smaller the number of detailed analyses required.[4] Some very effective approximations have been developed in the structures area,[3] the most successful ones based on insight into the physical and mathematical nature of structural analysis problems. In other areas necessary for aeroservoelastic synthesis, some promising approximations have been examined,[11] but in the area of wing/control surface unsteady aerodynamics[12] no such approximations are yet available.

Practically all of the work to date in the area of aeroservoelastic synthesis has been limited to sizing-type design variables. With a given planform shape, unsteady aerodynamic influence coefficient matrices can be calculated only once, and variations in generalized aerodynamic forces depend only on mode shape variations caused by changes in structural sizing design variables. If fixed modes are used,[13] a constant matrix of generalized unsteady aerodynamic forces can be used throughout the design optimization process.

In conceptual and preliminary design, however, airplane shape variations should be considered before the shape of a configuration is frozen. Generalized unsteady forces need to be updated because of changes in wing planform. These generalized aerodynamic forces have to be evaluated at several reduced frequencies, spanning the reduced frequency range of interest. Rational function approximations are then fitted in the frequency domain, so that linear time invariant (LTI) state–space models can be constructed and used for modern control synthesis techniques.[12]

The challenge associated with planform shape optimization is not only because of the intensive computation required for the generation, but also because of time and again, and for many reduced frequencies, of unsteady loads on wings and control surfaces. Effective approximation techniques, as required by NLP/AC, are still unavailable. Linear and reciprocal Taylor-series-based approximations perform generally quite poorly.[12] Analytic sensitivities of unsteady loads with respect to planform shape and control surface size and locations are required. In addition, recent experience shows that techniques of steady aerodynamics, when used for wing-shape optimization, may lead to nonsmooth behavior with respect to changes in shape design variables.[14] Such nonsmoothness, when in the context of analysis only (when only a few predictions of aerodynamic characteristics are required), presents no difficulty since only very small fluctuations of predicted results are observed. However, when used for optimization studies these small fluctuations in analysis results may lead to large fluctuations in the value of derivatives with respect to shape, adversely affecting the convergence of the optimization process.

The development of design-oriented unsteady aerodynamic analysis for wings and control surfaces in subsonic flight has been presented in Ref. 12. It was guided by the desire to find a modeling technique based on simple, explicit formulations, making it possible to derive analytic sensitivities in closed form, and gain insight into the mathematical structure of the problem.

In this paper the work of Ref. 12 is extended to the supersonic speed regime. Analytic sensitivities of supersonic unsteady aerodynamic loads with respect to planform shape are derived for planar wing/control surface configurations. Smoothness of analysis results (in both subsonic and supersonic flows) is studied and some sources for nonsmooth behavior are identified and eliminated. New approximation techniques for unsteady aerodynamic loads are evaluated in terms of their accuracy and computational cost. The present work adds insight and experience, where the development of reliable approximation concepts is crucial to the success of multidisciplinary aeroservoelastic synthesis for the early stages of airplane design.

Design-Oriented Supersonic Unsteady Aerodynamics for Planar Wing/Control Surfaces

Techniques for the computation of unsteady aerodynamic forces on combinations of lifting surfaces and bodies have reached a certain maturity in the past several years.[15,16] Effective panel (lattice) methods and assumed pressure methods for planar and nonplanar lifting surfaces have both been found to correlate quite well with experiments for subsonic and supersonic wings in attached, small disturbance flow, and have become standard tools in industry, with application to a wide range of airplane configurations.[17] Using assumed pressure-solution techniques, analytic sensitivities with respect to shape have been derived in Refs. 18 and 19 for wings. Using the subsonic doublet point method (DPM)[20,21] for planar wing/control surface configurations, analytic sensitivities with respect to planform and control surface shape have been derived in Ref. 12 for the subsonic case. The subsonic DPM offers a formulation in which aerodynamic influence coefficients are simple to evaluate, exposing the relations between unsteady aerodynamic pressures and wing/control surface shape, and making it possible to obtain analytic sensitivities explicitly.

In an effort to gain similar insights, leading to analytic sensitivities and approximations for supersonic wings and control surfaces, a similar method was sought. Desirable properties included simplicity of formulation and computational efficiency, together with adequate accuracy for flutter and aeroservoelastic analysis of real airplanes. The supersonic DPM[22,23] was such a candidate. However, in some test cases, oscillatory pressure distributions were reported with this method. Also in the supersonic DPM a branching process is used to determine the downwash on an averaging downwash area, depending on how that averaging area is cut by Mach lines from the sending doublet. There was a concern that these would lead to more severe nonsmooth behavior of the predicted generalized forces[14] than is inherent to the problem.

The design-oriented supersonic aerodynamic analysis of planar wing/control surface configuration developed here is based on the ideas presented in Refs. 22–26. In the planar case, the integral equation relating nondimensional pressure to nondimensional downwash on a combination of lifting surfaces is

$$w(x, y) = \frac{1}{8\pi} \int \int_{\Sigma} \Delta p(\xi, \eta) K(x_0, y_0)\, d\xi\, d\eta \tag{1}$$

where the supersonic kernel is given by[22]

$$K(x_0, y_0) = e^{-i\hat{k}x_0} \left\{ \frac{M^2}{R} \left(\frac{e^{-i\hat{k}X_1}}{x_0 + X_1} + \frac{e^{-i\hat{k}X_2}}{x_0 + X_2} \right) + \int_{X_1}^{X_2} \frac{e^{-i\hat{k}\nu}}{(y_0^2 + \nu^2)^{3/2}}\, d\nu \right\} \tag{2}$$

Σ is the area surrounded by the upstream Mach cone originating at the receiving point (x, y), and $x_0 = x - \xi$, $y_0 = y - \eta$, $R = \sqrt{x_0^2 - \beta^2 y_0^2}$

$$X_1 = (x_0 - MR)/\beta^2 \quad X_2 = (x_0 + MR)/\beta^2 \quad \beta = \sqrt{M^2 - 1}$$

The wing (or combination of wings) is divided into trapezoidal elements with sides parallel to the flow. The pressure on each trapezoid is assumed constant. The integral equation is written in discrete form, with the element pressures $\{\Delta \boldsymbol{p}_k\}$ as unknowns

$$w(x_j, y_j) = \frac{1}{8\pi} \sum_{k=1}^{N} \Delta p_k \left[\int \int_{\sigma_k} K(x_j - \xi, y_j - \eta)\, d\xi\, d\eta \right] = \frac{1}{8\pi} \sum_{k=1}^{N} \Delta p_k \cdot (\bar{K} \cdot K_0)_{jk} \tag{3}$$

The kernel is now expressed as a product of a steady part and an unsteady factor.[22–25] The unsteady factor and steady part are expressed as, respectively,

$$\bar{K}_{jk} = \bar{K}(x_j - \bar{\xi}_k, y_j - \bar{\eta}_k) = \bar{K}(\bar{x}_0, \bar{y}_0) \tag{4}$$

$$(K_0)_{jk} = \int\int_{\sigma'_k} \frac{2x_0}{y_0^2\sqrt{x_0^2 - \beta^2 y_0^2}}\,\mathrm{d}x_0\,\mathrm{d}y_0 \tag{5}$$

where σ'_k denotes the part of the element area of σ_k inside the forward Mach cone with apex at (x_j, y_j). The summation is carried out only for those sending elements submerged totally or partially in the Mach cone, since the influence coefficient $(\bar{K}\cdot K_0)_{jk}$ is zero for a sending element completely outside the Mach cone. The unsteady factor is written as

$$\bar{K}_{jk} = e^{-i\hat{k}\bar{x}_0}\left[\frac{M^2\bar{y}_0^2}{2\bar{x}_0}\left(\frac{e^{-i\hat{k}\bar{X}_1}}{\bar{x}_0 + \bar{X}_1} + \frac{e^{-i\hat{k}\bar{X}_2}}{\bar{x}_0 + \bar{X}_2}\right) + \frac{R\bar{y}_0^2}{2\bar{x}_0}\int_{\bar{X}_1}^{\bar{X}_2}\frac{e^{-i\hat{k}\nu}}{(\bar{y}_0^2 + \nu^2)^{3/2}}\,\mathrm{d}\nu\right]$$

$$\bar{X}_1 = X_1(\bar{x}, \bar{y}), \qquad \bar{X}_2 = X_2(\bar{x}, \bar{y}) \tag{6}$$

which is evaluated at the centroid of the integration area of the kth element. When the element is completely inside the forward Mach cone of the upwash point, the coordinates of the centroid are (Fig. 1)

$$\begin{aligned}\bar{x}_0 = \frac{1}{6\sigma_k}\,[&(x_{01} + x_{02})(y_{01}x_{02} - y_{02}x_{01}) \\ &+ (x_{02} + x_{03})(y_{02}x_{03} - y_{03}x_{02}) \\ &+ (x_{03} + x_{04})(y_{03}x_{04} - y_{04}x_{03}) \\ &+ (x_{04} + x_{01})(y_{04}x_{01} - y_{01}x_{04})]\end{aligned} \tag{7}$$

$$\begin{aligned}\bar{y}_0 = \frac{1}{6\sigma_k}\,[&(y_{01} + y_{02})(y_{01}x_{02} - y_{02}x_{01}) \\ &+ (y_{02} + y_{03})(y_{02}x_{03} - y_{03}x_{02}) \\ &+ (y_{03} + y_{04})(y_{03}x_{04} - y_{04}x_{03}) \\ &+ (y_{04} + y_{01})(y_{04}x_{01} - y_{01}x_{04})]\end{aligned} \tag{8}$$

with $y_{01} = y_{04}$ and $y_{02} = y_{03}$.

The steady factors $(K_0)_{jk}$ are formulated as functions of coordinates of the four corner points of kth sending element in the following form:

$$\begin{aligned}(K_0)_{jk} = {} & F(x_{01}, y_{01}, S_{12}) - F(x_{02}, y_{02}, S_{12}) \\ & + F(x_{03}, y_{03}, S_{34}) - F(x_{04}, y_{04}, S_{34})\end{aligned} \tag{9}$$

where the function $F(x_0, y_0, S)$, depending on whether S is smaller or greater than β, is given by

$$F(x_0, y_0, S) = -\frac{2}{y_0}\sqrt{x_0^2 - \beta^2 y_0^2} - 2S\,\ell n\left(\frac{x_0 + \sqrt{x_0^2 - \beta^2 y_0^2}}{\beta|y_0|}\right) + \begin{cases} -2\sqrt{\beta^2 - S^2}\,\arcsin\left[\dfrac{\beta^2 y_0 - Sx_0}{\beta(x_0 - Sy_0)}\right] & |S| < \beta \\ 0 & |S| = \beta \\ 2\sqrt{S^2 - \beta^2}\,\ell n\left|\dfrac{\beta^2 y_0 - Sx_0 - \sqrt{(S^2 - \beta^2)(x_0^2 - \beta^2 y_0^2)}}{\beta(x_0 - Sy_0)}\right| & |S| > \beta \end{cases} \tag{10}$$

and the sweeps of the leading edge $\overline{12}$ and trailing edge $\overline{34}$ of each trapezoidal element are

$$\begin{aligned}S_{12} &= (x_{01} - x_{02})/(y_{01} - y_{02}) \\ S_{34} &= (x_{03} - x_{04})/(y_{03} - y_{04})\end{aligned} \tag{11}$$

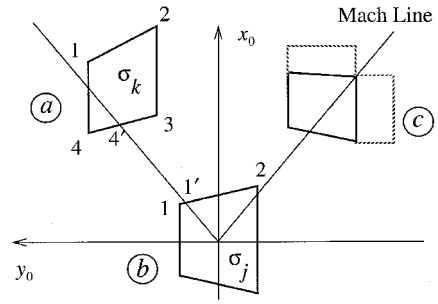

Fig. 1 Sending and receiving elements.

The previous formulation is still valid when the Mach line crosses the kth element, but the points outside of the Mach cone have to be replaced by the intersection points on the leading or trailing edges of the element, so that pressures outside of the Mach cone do not contribute to downwash at the receiving point $(x_0 = 0, y_0 = 0)$. For example, in Fig. 1 the Mach line intersects the trailing edge of element a at point (x'_{04}, y'_{04}), then

$$\begin{aligned}K_{jk} = {} & F(x_{01}, y_{01}, S_{12}) - F(x_{02}, y_{02}, S_{12}) \\ & + F(x_{03}, y_{03}, S_{34}) - F(x'_{04}, y'_{04}, S_{34})\end{aligned} \tag{12}$$

If the sending element is crossed by the Mach line, the integration area does not cover the whole trapezoidal shape. The formulations of $(\bar{x}_0, \bar{y}_0)$ for the evaluation of the unsteady factors are modified to take only the actual integration area within the Mach cone into account. Explicit, simple expressions for $(\bar{x}_0, \bar{y}_0)$ are available for these cases also.

Because $\bar{K}$ is singular at the point $x_0 = 0$, a special treatment is required when the sending element is the same as the receiving element (element b in Fig. 1). Following Ref. 22, the unsteady kernel is expanded in terms of reduced frequency

$$K(x_0, y_0) = \frac{2x_0}{Ry_0^2}\left[1 - i\hat{k}\left(x_0 + \frac{y_0^2}{x_0}\right) - \frac{\hat{k}^2}{2} \times \left(x_0 + \frac{2M^2 - 1}{\beta^2}y_0^2 + \frac{Ry_0^2}{2x_0}\,\ell n\,\frac{x_0 + R}{x_0 - R}\right) + \cdots\right] \tag{13}$$

As $y_0 = 0$ and x_0 approaches zero, the term $-2i\hat{k}/R$ is not small, and the unsteady factor cannot be taken as constant over the element area. As in Ref. 22, the integration of the term $-2i\hat{k}/R$ is added to create an average $\bar{K}_{jk}$ when evaluating the influence coefficients for $(x_0 = 0, y_0 = 0)$. The integration of $-2i\hat{k}/R$ can be formulated as

$$\begin{aligned}I_j &= \int\int\left(-\frac{2i\hat{k}}{R}\right)\mathrm{d}x_0\,\mathrm{d}y_0 \\ &= -2i\hat{k}\{\boldsymbol{G}(x_{02}, y_{02}) - \boldsymbol{G}(x_{01}, y_{01})\}\end{aligned} \tag{14}$$

where (x_{01}, y_{01}) and (x_{02}, y_{02}) are the corner points of the leading edge of the element if the whole line is inside the Mach cone. If a corner point is outside of the Mach cone, it is replaced by the intersection point of the leading edge and the Mach line (Fig. 1). The integral should then be

$$G(x_0, y_0) = y_0 \ell n \frac{x_0 + R}{|\beta y_0|} + \begin{cases} \dfrac{x_0 - S_{12}y_0}{\sqrt{\beta^2 - S_{12}^2}} \arcsin\left[\dfrac{\beta^2 y_0 - S_{12}x_0}{\beta(x_0 - S_{12}y_0)}\right] & |S_{12}| < \beta \\ 0 & |S_{12}| = \beta \\ \dfrac{x_0 - S_{12}y_0}{\sqrt{S_{12}^2 - \beta^2}} \ell n \left|\dfrac{\beta^2 y_0 - S_{12}x_0 - R\sqrt{(S_{12}^2 - \beta^2)}}{\beta(x_0 - S_{12}y_0)}\right| & |S_{12}| > \beta \end{cases} \quad (15)$$

$$I_j = -2i\hat{k}\{\boldsymbol{G}(x_{02}, y_{02}) - \boldsymbol{G}(x_{01'}, y_{01'})\} \quad (16)$$

The equations relating nondimensional upwash to nondimensional pressure differences on a set of trapezoidal elements is

$$8\pi w_j = \sum_{k=1}^{n} A_{jk} \cdot f_k \quad (17)$$

where

$$f_k = \Delta p_k \sigma_k \quad (18)$$

$$A_{jk} = \begin{cases} (\bar{K}K_0)_{jk}/\sigma_k & k \neq j \\ [(\bar{K}K_0)_{jk} + I_j]/\sigma_k & k = j \end{cases} \quad (19)$$

Equations for $(K_0)_{jk}$ and $\bar{K}_{jk}$ are explicit and simple to evaluate, except for the integral in Eq. (6)

$$\int_{X_1}^{X_2} \frac{e^{-i\hat{k}\nu}}{(y_0^2 + \nu^2)^{3/2}} \, d\nu$$

which is evaluated using the expansion series of Refs. 22 and 27. Generalized aerodynamic forces, associated with downwash caused by motion in mode n

$$[A]\{\boldsymbol{f}\}_n = 8\pi\{\boldsymbol{w}\}_n \quad (20)$$

and generalized displacement m (mode shape $\{\boldsymbol{h}\}_m$) can now be obtained from

$$Q_{m,n} = \{\boldsymbol{h}\}_m^T\{\boldsymbol{f}\}_n \quad (21)$$

Analytic Sensitivities with Respect to Planform Shape

When fixed shape generalized coordinates (deformation functions) defined in the global (x, y) axes are used, then upwash and displacement at a panel control point depend only on the location of that point in the global axes. For example, simple polynomial Ritz functions can be used in the equivalent plate structural wing modeling method,[28] or to fit finite element displacements given on a finite element grid.[29]

A typical deformation mode, j, $x^{p_j}y^{q_j}$, is then given as a set of displacements at control points over the aerodynamic grid, in a vector

$$\begin{Bmatrix} \cdots \\ \boldsymbol{h}_k \\ \cdots \end{Bmatrix}_j = (\boldsymbol{x}k)^{p_j}(\boldsymbol{y}k)^{q_j} \quad (22)$$

The location of element control points in terms of planform shape design variables, used to parameterize the shape of the planform and size and location of control surfaces, can be given explicitly by

$$x_k = x_k(DV_l) \qquad y_k = y_k(DV_l) \quad (23)$$

Where DV_l are shape design variables. The explicit expressions for elements of the aerodynamic influence coefficient matrix [Eq. (17)], as well as expressions for areas of trapezoidal elements, upwash on elements and displacements on elements, all make it possible to obtain analytic sensitivities of the unsteady aerodynamic forces with respect to planform shape DV_l explicitly.

Eq. (17) is differentiated as follows:

$$[A]\left\{\frac{\partial f}{\partial \boldsymbol{DV}}\right\} = 8\pi\left\{\frac{\partial \boldsymbol{w}}{\partial \boldsymbol{DV}}\right\} - \left[\frac{\partial A}{\partial DV}\right]\{\boldsymbol{f}\} \quad (24)$$

Since an L–U decomposition of the coefficient matrix is available from the analysis step, the analytical shape sensitivity solutions correspond to new right-hand sides, and involve only forward and backward substitutions.

Normalized downwash at a point (x, y), because of a mode shape $x^p y^q$, is given by

$$i\hat{k}\frac{x^p y^q}{b} + \frac{\partial}{\partial x}(x^p y^q) = i\hat{k}\frac{x^p y^q}{b} + p(x^{p-1}y^q) = w(x, y) \quad (25)$$

and for mode (displacement shape function) i, this can be differentiated with respect to planform design variables

$$\frac{\partial}{\partial DV} w_i(x_k, y_k) = \frac{\partial w_i \partial x_k}{\partial x_k \partial DV} + \frac{\partial w_i \partial y_k}{\partial y_k \partial DV} \quad (26)$$

$\bar{K}_{ij}$ depends, in general, on the distance between the area centroids of sending and receiving points [Eqs. (6–8)]. The steady part $(K_0)_{ij}$ obtained by integration over the area of a sending element depends on the (x, y) coordinates of the relative distances of the vertices of that area from the upwash point [Eqs. (9–11)]. Similarly, the area of the sending element also depends on the coordinates of those vertices.

Since the topology of the mesh is not changed and every point of the mesh is linked explicitly to the overall shape DV [Eq. (23)], then by chain rule differentiation it is possible to obtain analytic sensitivities of the aerodynamic influence coefficients with respect to planform shape DV. Explicit expressions for those analytic sensitivities are listed in the Appendix. Note that when the sending trapezoid is crossed by a Mach line from the receiving point, coordinates of the Mach line intersections with the element depend on the relative position of the element with respect to the receiving point. As the mesh changes because of changes in DV, sensitivities of the intersection point location with respect to DV can be calculated. In certain situations, this leads to a discontinuity in the shape derivatives of the contribution of a sending element, at points where, because of changes of the mesh, an intersection point moves from one side of the element to the neighboring side. In Fig. 1, element C is in such a position. As far as integration of the steady part of the kernel over the sending area is concerned, this discontinuity is somewhat offset by the contribution of the neighboring element, where the intersection point also moves from one side to another, to compensate for the change in the first element. Differences in pressure on the two neighboring elements and different unsteady factors contribute to an overall discontinuous derivative in such a situation. However, when only a few elements are involved, the overall effect on planform shape sensitivity is expected to be small.

This does not apply, of course, to situations in which overall Mach line patterns change over the configuration. Among many possibilities, an example here is a case in which for some reference planform shape the Mach line is exactly on the leading edge of a wing. As the aspect ratio is changed, or the sweep of the leading edge, the leading edge becomes either

subsonic or supersonic, depending on the direction of change. In such cases, discontinuous shape derivatives are expected and reflect the physical nature of the problem.

Subsonic Analytic Sensitivities

The supersonic capability described previously complements the subsonic capability, based on the subsonic DPM, discussed in Ref. 12. With explicit formulations and analytic-shape sensitivities available for wing/control surface configurations in unsteady subsonic and supersonic flow, attention can now be focused on issues of smooth/nonsmooth behavior (Ref. 14) and the search for effective approximation concepts.

Alternative Approximations: Taylor-Series-Based Approximations

The limitations of Taylor-series-based unsteady aerodynamic direct and reciprocal approximations have already been exposed in Ref. 12 in the context of subsonic flow. These approximations are explicit and fast computationally and they are constructed based on the results of analysis and sensitivity analysis for a reference (base) configuration. In the direct case

$$Q_{m,n} = (Q_0)_{m,n} + \{\nabla \boldsymbol{Q}_{m,n}\}_0^T \{\boldsymbol{DV} - \boldsymbol{DV}_0\} \tag{27}$$

Approximation Based on Linear Perturbation

In an effort to obtain better approximations that allow larger move limits for NLP/AC-based optimization, two additional approximations are studied here. Both involve more computational effort than the direct and reciprocal Taylor-series approximations. The first is based on linear perturbation of the discretized lifting surface equations, where, to first order

$$[A]_0\{\Delta \boldsymbol{f}\} = 8\pi\{\Delta \boldsymbol{w}\} - [\Delta A]\{\boldsymbol{f}\}_0 \tag{28}$$

This is similar to the sensitivity equations [Eq. (24)], and only forward and backward substitutions are required for the variation in element forces. However, it is proposed in the present approximation that the changes in downwash and aerodynamic influence coefficient matrix will be calculated exactly. That is, with every variation of planform, a new downwash vector and a new aerodynamic influence coefficients matrix should be calculated, capturing more of the nonlinearities involved with shape changes. Because of the explicit formulation of downwash and $[A]$ matrix terms in both subsonic DPM and the present supersonic capability, such a computation is fast compared with other methods of solution in lifting surface theory. Thus,

$$[\Delta A] = [A] - [A]_0 \tag{29}$$

$$\{\Delta w\} = \{w\} - \{w\}_0 \tag{30}$$

and new approximated generalized forces are obtained using the exact new displacement vector $\{\boldsymbol{h}\}$, the new element areas, and the force vector $\{\boldsymbol{f}_0 + \Delta \boldsymbol{f}\}$.

Second-Order Approximation

The adjoint set of discretized lifting surface equations and reverse flow theorems have been used in the past[30,31] to determine optimal positions of collocation points, to extrapolate unsteady aerodynamic forces from coarse grids to finer grids, or to calculate accurate unsteady aerodynamic loads in cases in which the reverse flow problem is simpler than the direct flow problem. In an application of the same principles to approximation concepts for NLP/AC, a new approximation technique for generalized aerodynamic loads with second-order accuracy is developed as follows:

Let the discretized lifting surface system of equations be

$$[A]\{\boldsymbol{f}\}_n = 8\pi\{\boldsymbol{w}\}_n \tag{31}$$

and the generalized force associated with deformation mode m and downwash mode n

$$Q_{m,n} = \{\boldsymbol{h}\}_m^T\{f\}_n = 8\pi\{\boldsymbol{h}\}_i^T[A]^{-1}\{\boldsymbol{w}\}_j \tag{32}$$

An adjoint solution vector can now be introduced so that

$$Q_{m,n} = \{\boldsymbol{\eta}\}_m^*\{\boldsymbol{w}\}_n = 8\pi\{\boldsymbol{h}\}_m^T[A]^{-1}\{\boldsymbol{w}\}_n \tag{33}$$

Thus, the equation for the adjoint vector is

$$[A]^*\{\boldsymbol{\eta}\}_m = 8\pi\{\boldsymbol{h}\}_m \tag{34}$$

As Eqs. (32) and (33) show, the generalized force can be obtained using either the direct solution [Eq. (31)] or the adjoint solution [Eq. (34)]. As Ref. 31 shows, if approximations are available for the direct and adjoint vectors $\{\boldsymbol{f}\}$ and $\{\boldsymbol{\eta}\}$, then an approximation with second-order accuracy can be obtained for the generalized force in the form

$$\tilde{Q}_{m,n} = \{\boldsymbol{h}\}_m^T\{\tilde{\boldsymbol{f}}\}_n + \{\tilde{\boldsymbol{\eta}}\}_m^*\{\boldsymbol{w}\}_n - (1/8\pi)\{\tilde{\boldsymbol{\eta}}\}_m^*[A]\{\tilde{\boldsymbol{f}}\}_n \tag{35}$$

or in an alternative formulation, insensitive to the scale of the approximate $\{\tilde{\boldsymbol{\eta}}\}$, $\{\tilde{\boldsymbol{f}}\}$ vectors:

$$\tilde{Q}_{m,n} = 8\pi \frac{\{\boldsymbol{h}\}_m^T\{\tilde{\boldsymbol{f}}\}_n \cdot \{\tilde{\boldsymbol{\eta}}\}_m^*\{\boldsymbol{w}\}_n}{\{\tilde{\boldsymbol{\eta}}\}_m^*[A]\{\tilde{\boldsymbol{f}}\}_n} \tag{36}$$

The influence coefficient matrix $[A]$ together with downwash and displacement vectors are newly evaluated at each new design point. However, Eq. (31) is not solved again for new planforms. The direct and adjoint solutions at the reference configuration are now used as approximate solutions in Eq. (36), leading to a second-order approximation of the associated generalized load.

It is interesting to compare the computational effort required in this approximation with that of a detailed analysis. If N aerodynamic elements (trapezoids) are used in the mesh over the configuration and M deformation modes, then (counting floating point operations, flops,[32] excluding the regeneration of the $[A]$ matrix and the downwash and displacement vectors) the total number of complex flops in a complete solution is[32,34]

$$2N^3/3 + 2N^2M + 2NM^2 \tag{37}$$

Using the approximation of Eq. (36), with direct and adjoint solutions from the reference (base) design point, the number of complex flops is calculated to be

$$2N^2M + 2NM^2 + 4NM^2 + 2M^2 \tag{38}$$

Comparing the operation counts in Eqs. (37) and (38), it is found that substantial savings can be materialized if the number of displacement mode shapes is small with respect to the number of aerodynamic elements. This is usually the case with panel and lattice methods. For instance, if 20 modes and 200 panels are used, the computational effort associated with the second-order approximation is 29.3% of the effort needed for complete solution. If 20 modes and 400 panels are used, or 10 modes and 200 panels, then the second-order approximation requires only 14.9% of the computational effort required for complete solution. These counts do not include the generation of new aerodynamic influence coefficient matrices, downwash vectors, and deformation vectors, an effort that is identical whether a complete solution or second-order approximation is used. Comparison of CPU times required for a complete detailed solution and a second-order approximation (including the generation of the A matrix) on a DEC Alpha workstation

shows that, with 20 modes and 400 aerodynamic boxes on a 60-deg swept wing at $M = 1.44$, the second-order approximation takes 42% as long as the complete solution (17.1 vs 40.2 s). When the number of boxes is increased to 900, the second-order approximation takes 83.35 s, compared with 349.35 s for the detailed analysis, a savings of 76%.

If major improvements in accuracy over the standard Taylor-series-based approximations are obtained with the second-order approximation, it should be seriously considered for wing-shape optimization with NLP/AC, despite the added computational burden.

Test Cases

A series of test cases are used here to examine different aspects of the techniques and issues discussed in this work. First, the accuracy of the design-oriented supersonic unsteady aerodynamic capability, as developed here, is studied by application to four wing cases taken from Refs. 22, 33, and 35. The configurations studied are the rectangular wing (AR = 2) and the 60-deg swept wing (AR = 1.85) used in Ref. 22, as well as the AGARD wing–tail configuration (Fig. 2) and AGARD wing/control surface configuration (Fig. 3). Steady and unsteady pressure distributions as well as generalized aerodynamic forces with and without control surfaces are studied.

Studies of the smoothness of unsteady aerodynamic predictions in both subsonic and supersonic flows follow. Accuracy of the alternative approximation techniques discussed was also examined in subsonic as well as supersonic cases.

Results

Steady pressure distributions on the 60-deg swept wing at $M = 1.44$ (Fig. 4), the AGARD wing–tail configuration at $M = 1.2$ (Fig. 5), and the rectangular wing at $M = 1.2$ (Ref. 33) show good correlation with analytic, assumed pressure,[35] and doublet point results and no oscillatory behavior. The case of the AGARD wing–tail configuration is interesting, because with the same coarse mesh, the supersonic doublet point method yields oscillatory pressures near the leading edge, whereas results obtained with the present capability show no such oscillation. Comparison of unsteady aerodynamic forces

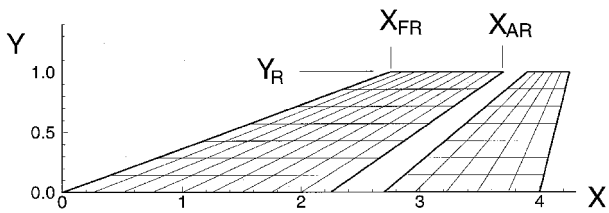

Fig. 2 AGARD wing–tail configuration (14 × 7 grid).

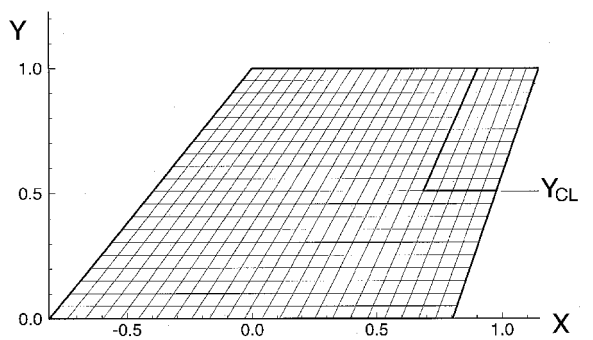

Fig. 3 AGARD wing/control surface configuration (23 × 20 grid).

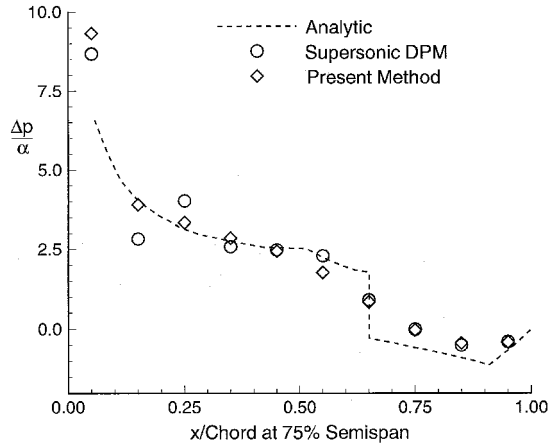

Fig. 4 Steady pressure on the 60-deg swept wing at 75% semispan ($M = 1.44$).

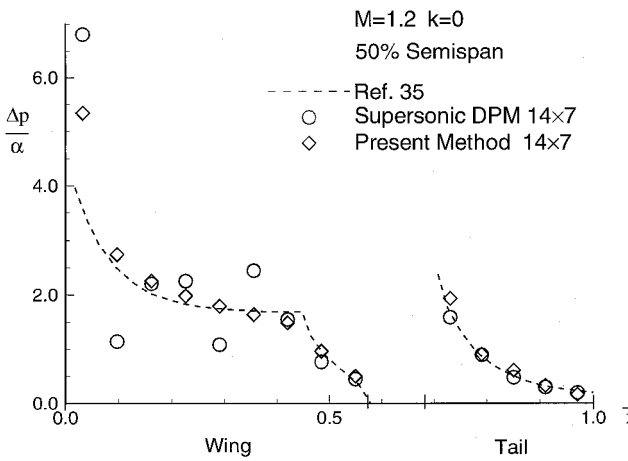

Fig. 5 Steady pressure on the AGARD wing–tail configuration at 50% semispan ($M = 1.2$, results obtained with 14 × 7 grid).

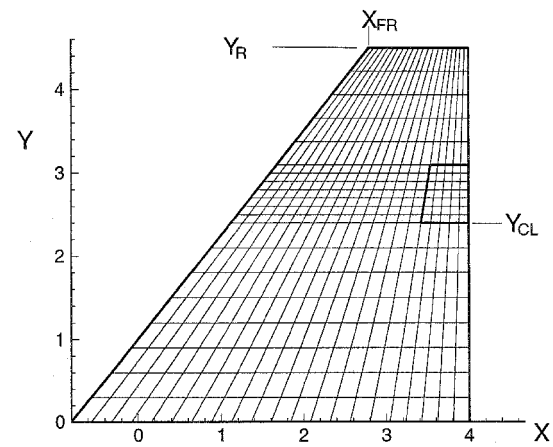

Fig. 6 Fighter-type wing with control surface (21 × 20 grid).

obtained using the present capability with results from other methods for the AGARD wing–tail configuration is given in Ref. 33. Comparisons of unsteady aerodynamic forces for the AGARD wing/control surface configuration are shown in Table 1. In all cases, the present capability performs well.

With confidence in the reliability of the design-oriented supersonic capability developed here and the subsonic DPM[12,20] for interfering planar wings and wing/control surface configurations, issues of concern for MDO applications, the main thrust of the present work, can now be addressed.

Table 1 Generalized forces of the AGARD tapered swept-back wing/control surface configuration

		$\mathrm{Re}[Q_{i,j}]$			$\mathrm{Im}[Q_{i,j}]/k$		
i	j	Method 9[a]	Method 19[a]	Present	Method 9[a]	Method 19[a]	Present
1	1	0.092	0.05753	0.01275	2.426	2.35676	2.41350
1	2	2.498	2.42334	2.45431	0.698	0.69640	0.77476
1	3	1.615	1.53169	1.57971	0.578	0.56087	0.63896
1	4	−0.067	−0.07017	−0.08498	0.626	0.57108	0.59942
1	5	0.284	0.28064	0.26291	0.020	0.02434	0.03232
2	1	−0.100	−0.11323	−0.10793	0.422	0.39447	0.38198
2	2	0.505	0.47387	0.43905	0.845	0.82809	0.84785
2	3	1.494	1.42893	1.46799	0.260	0.24737	0.30550
2	4	−0.085	−0.08105	−0.08480	0.175	0.15194	0.15453
2	5	0.266	0.25941	0.24172	0.021	0.02391	0.03097
3	1	−0.087	−0.09637	−0.09962	0.502	0.48224	0.48805
3	2	0.554	0.53147	0.52636	0.508	0.49556	0.50943
3	3	0.852	0.80105	0.81116	0.308	0.28980	0.32380
3	4	−0.078	−0.07266	−0.07610	0.129	0.11363	0.11676
3	5	0.251	0.24205	0.22444	0.019	0.02362	0.02991
4	1[b]	0.024	0.00934	−0.08816	0.674	0.61908	0.64531
4	2[b]	0.656	0.60126	0.00063	0.287	0.26820	0.29432
4	3[b]	0.644	0.57210	0.61678	0.392	0.27538	0.31202
4	4[b]	−0.084	−0.07840	0.60107	0.295	0.25233	0.26836
4	5[b]	0.167	0.15660	0.15049	0.011	0.01336	0.01824
5	1	−0.012	−0.01286	−0.01190	0.018	0.01700	0.01525
5	2	0.021	0.01900	0.01694	0.040	0.03991	0.03752
5	3	0.056	0.05343	0.05005	0.026	0.02568	0.02463
5	4	−0.010	−0.00972	−0.00917	0.007	0.00566	0.00517
5	5	0.036	0.03495	0.02898	0.004	0.00512	0.00508

[a]Results are reported in Ref. 33.
[b]Present results match Ref. 33 results in a switched order. It seems that Ref. 33 results for $\mathrm{Re}[Q_{4,j}]$ are printed in the wrong order.

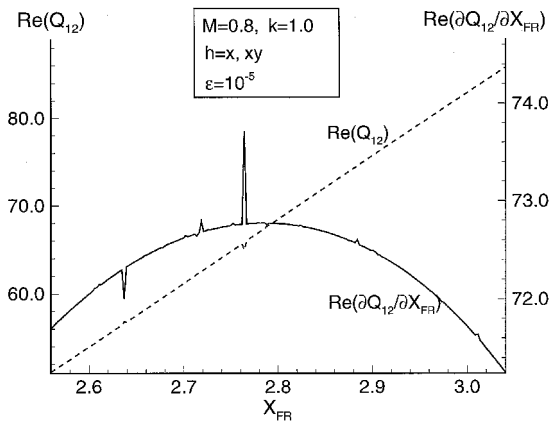

Fig. 7 Nonsmooth variation of the real parts of a subsonic generalized force $Q(x, xy)$ and its sensitivity $\partial Q/\partial X_{FR}$ as a function of the x coordinate of the tip leading edge X_{FR} (Fig. 4), convergence = 10^{-5} for the Ueda series (* normalized by their absolute values at $X_{FR} = 2.8$).

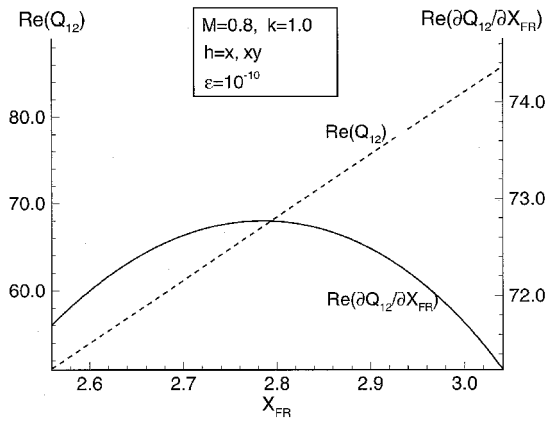

Fig. 8 Variation of the real parts of a subsonic generalized force $Q(x, xy)$ and its sensitivity as a function of X_{FR} (Fig. 4), convergence = 10^{-10} for the Ueda series (* normalized by their absolute values at $X_{FR} = 2.8$).

Sample results of a parametric study of the subsonic fighter-type wing (Fig. 6) to examine the smoothness of aerodynamic results, in the light of the findings of Ref. 14, are shown in Figs. 7 and 8. The x coordinate of the wing-tip leading-edge point X_{FR} was changed from the reference value of 2.8 m, with 200 points covering the range shown. Examination of the real and imaginary parts of the subsonic $Q(x, xy)$ shows nonsmooth behavior of the generalized force and its shape sensitivity (real parts shown in Fig. 7). The fluctuations in analysis predictions of the generalized force itself are very small. When used in shape optimization, however, the jumps in derivative can hurt optimization process convergence or lead the resulting design to reside in a local minimum that has no physical meaning.

An investigation into the source of the numerical fluctuations in subsonic flow cases was conducted and the cause was found in the series evaluation of the B function in the kernel[22,27]:

$$B(k, y_0, X) = \int_{-\infty}^{X} \frac{e^{i\hat{k}\nu}}{(y_0^2 + \nu^2)^{3/2}}\, d\nu$$

$$= B_R(\hat{k}, y_0, X) + iB_I(\hat{k}, y_0, X)$$

Tightening the convergence criterion used in this series evaluation led to elimination of the nonsmooth behavior and smooth results were then obtained (Fig. 8).

In the supersonic case, conducted on the AGARD wing, no nonsmooth behavior was found. Since only a small increase in computational effort was noticed when convergence criterion were tightened, all results for supersonic cases were obtained with a convergence criteria of 10^{-5} (Fig. 9).

The present design-oriented capabilities, in both the subsonic and supersonic flow regimes, provide smooth predictions of unsteady aerodynamic loads with respect to planform shape. It is interesting to note that even in the supersonic case, where individual trapezoids may move into and out of the forward Mach cone (or be cut on different sides by a Mach line as they move) the predicted generalized forces seem to be quite smooth. The smearing of pressure predictions along planform Mach lines by a panel method, which cannot capture pressure gradient discontinuities the way an assumed pressure method can,[35,36] is probably a contributor to this smooth behavior.

The rest of the results shown here are used to assess the performance of the alternative approximation techniques discussed previously. Figure 10 shows a sample of the comparison of linear Taylor-series, linear-perturbation, and second-order approximations used for a unsteady subsonic case, where the wingtip is moved in a spanwise direction (Y_R).

For the AGARD wing in Fig. 2, supersonic approximations are compared in Fig. 11 for the case in which the wing tip is moved spanwise (the tail is not included in the calculation). The accuracy of the second-order approximation (based on the direct and adjoint solutions at the reference design) is very good over quite large move limits.

Results of parametric studies, where a control surface is increased and decreased in size (Fig. 4), are shown in Fig. 12 for the subsonic fighter wing case. The supersonic studies involving the control surface (Fig. 3) are shown in Figs. 13 and 14. In our case, the effect of control surface size on the resulting generalized forces is almost linear. The linear Taylor-series-approximation performs very well in this case. The second-order approximation performs quite well when real parts of generalized forces are approximated. Its accuracy deteriorates when imaginary parts (damping) are involved. The magnitude of these terms, however, is small compared with the generalized force terms for this wing. It is felt that additional studies are needed to understand this deterioration of performance. Additional results can be found in Ref. 34.

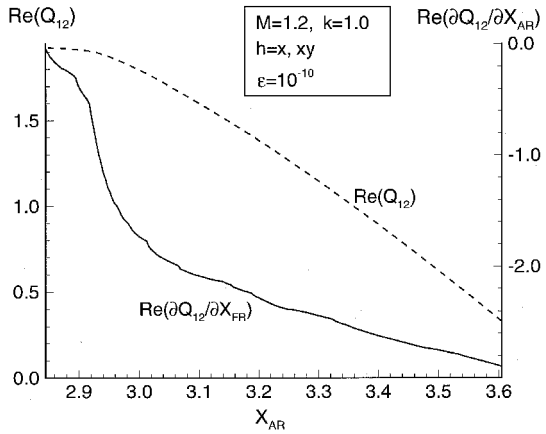

Fig. 9 Variation of the real parts of a supersonic generalized force $Q(x, xy)$ and its sensitivity $\partial Q/\partial X_{AR}$, as a function of the x coordinate of the tip trailing edge X_{AR} (Fig. 2, wing only), convergence = 10^{-10}.

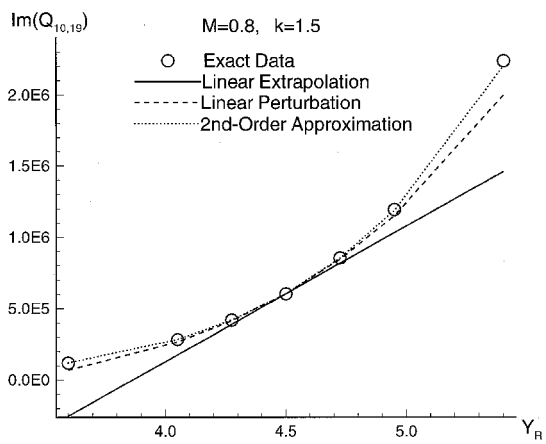

Fig. 10 Alternative approximations. Fighter-type wing (Fig. 4), variation of Y_R, unsteady subsonic flow (k = 1.5, M = 0.8), Im[$Q(y^3, x^2y^3)$].

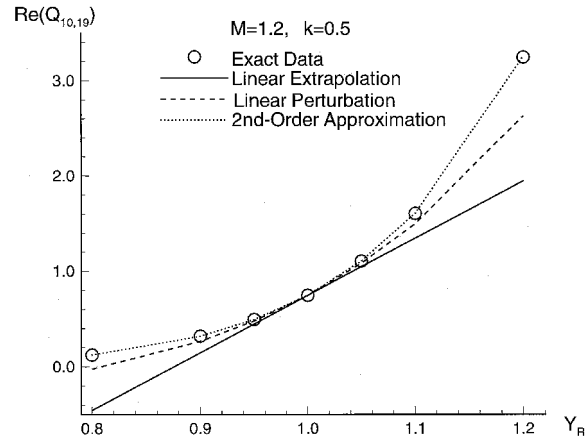

Fig. 11 Alternative approximations. AGARD wing (Fig. 2, wing only), variation of Y_R, unsteady supersonic flow (k = 0.5, M = 1.2), Re[$Q(y^3, x^2y^3)$].

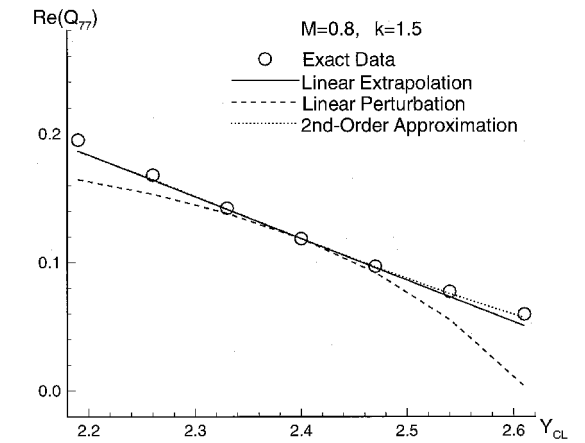

Fig. 12 Alternative approximations. Fighter wing/control surface (Fig. 4), variation of Y_{CL}, unsteady subsonic flow (k = 1.5), Re[hinge moment], M = 0.8.

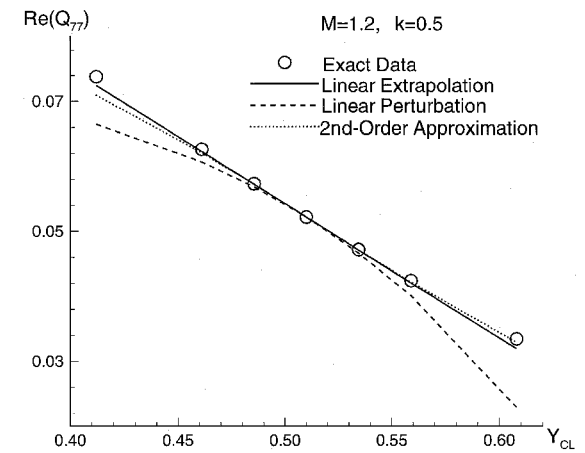

Fig. 13 Alternative approximations. AGARD wing/control surface (Fig. 3), variation of Y_{CL}, unsteady flow (k = 0.5), Re[hinge moment], M = 1.2.

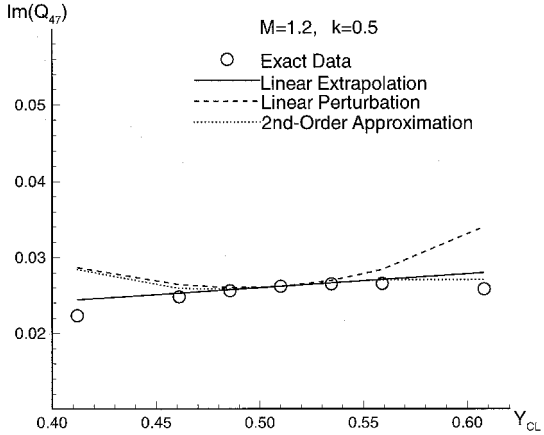

Fig. 14 Alternative approximations. AGARD wing/control surface (Fig. 3), variation of Y_{CL}, unsteady flow (k = 0.5), Im[$Q(x^2, \delta)$], M = 1.2.

The development of robust approximations for aerodynamic loads will be pursued and discussed in future works; it is the capability to effectively model and accurately approximate unsteady aerodynamics forces on a lifting surface/control surface configuration that will lead to the successful application of NLP/AC to planform shape optimization with active controls technology.

Conclusions

A design-oriented supersonic unsteady aerodynamic solution technique for wing/control surface combinations has been presented, complementing the subsonic capability presented previously. Explicit expressions for aerodynamic influence coefficients and upwash and deformation distributions made it possible to obtain analytic sensitivities with respect to planform shape in an efficient manner. Sources of analysis and derivative nonsmoothness were identified in both the subsonic and supersonic cases. They were traced to the series evaluation of part of the kernel, and, in the supersonic case, to changing patterns of Mach lines over trapezoidal elements and whole configurations. A second-order approximation technique, based on the direct and adjoint solutions at a design reference case, was introduced and shown to yield accurate predictions of unsteady air loads over move limits of up to 25%. The new capabilities and new approximations studied constitute part of the development of disciplinary tools required for configuration optimization of advanced airplanes with high authority active controls.

Appendix: Derivatives of the Supersonic Aerodynamic Matrix [A]

1) Differentiation of the aerodynamic influence coefficients [Eq. (19)]

$$A_{jk} = (\bar{K}K_0)_{jk}/\sigma_k \tag{A1}$$

$$\frac{\partial A_{jk}}{\partial DV} = \frac{1}{\sigma_k}\left[\bar{k}_{jk}\frac{\partial (K_0)_{jk}}{\partial DV} + (K_0)_{jk}\frac{\partial \bar{K}_{jk}}{\partial DV} - A_{jk}\frac{\partial \sigma_k}{\partial DV}\right] \tag{A2}$$

2) Planform shape sensitivity of the steady part $(K_0)_{jk}$

$$\frac{\partial (K_0)_{jk}}{\partial DV} = \frac{\partial}{\partial DV}F(x_{01}, y_{01}, S_{12}) - \frac{\partial}{\partial DV}F(x_{02}, y_{02}, S_{12}) + \frac{\partial}{\partial DV}F(x_{03}, y_{03}, S_{34}) - \frac{\partial}{\partial DV}F(x_{04}, y_{04}, S_{34}) \tag{A3}$$

where shape sensitivities of the function F are obtained from shape sensitivities of the relative distances of vertices of the sending element from the receiving element [Eqs. (9) and (10)]

$$\frac{\partial}{\partial DV}F(x_{0m}, y_{0m}, S) = \frac{\partial F}{\partial x_{0m}}\frac{\partial x_{0m}}{\partial DV} + \frac{\partial F}{\partial y_{0m}}\frac{\partial y_{0m}}{\partial DV} + \frac{\partial F}{\partial S}\frac{\partial S}{\partial DV} \qquad m = 1, 2, 3, 4 \tag{A4}$$

with

$$\frac{\partial F}{\partial x_{0m}} = -\frac{2\sqrt{x_{0m}^2 - \beta^2 y_{0m}^2}}{y_{0m}(x_{0m} - S y_{0m})} \tag{A5}$$

$$\frac{\partial F}{\partial y_{0m}} = \frac{2x_{0m}\sqrt{x_{0m}^2 - \beta^2 y_{0m}^2}}{y_{0m}^2(x_{0m} - S y_{0m})} \tag{A6}$$

$$\frac{\partial F}{\partial S} = \frac{2\sqrt{x_{0m}^2 - \beta^2 y_{0m}^2}}{(x_{0m} - S y_{0m})} - 2\,\ell n\left(\frac{x_{0m} + \sqrt{x_{0m}^2 - \beta^2 y_{0m}^2}}{\beta |y_{0m}|}\right) + \begin{cases} \dfrac{2S}{\sqrt{\beta^2 - S^2}} \arcsin\left[\dfrac{\beta^2 y_{0m} - S x_{0m}}{\beta(x_{0m} - S y_{0m})}\right] & |S| < \beta \\ \dfrac{-2S}{\sqrt{\beta^2 - S^2}}\,\ell n\left|\dfrac{\beta^2 y_{0m} - S x_{0m} - \sqrt{(S^2 - \beta^2)(x_{0m}^2 - \beta^2 y_{0m}^2)}}{\beta(x_{0m} - S y_{0m})}\right| & |S| > \beta \end{cases} \tag{A7}$$

$$\lim_{|S|\to\beta}\frac{\partial F}{\partial S} = 4\sqrt{\frac{x_{0m} + \beta y_{0m}}{x_{0m} - \beta y_{0m}}} \tag{A8}$$

The geometric terms $\partial x_{0m}/\partial DV$ and $\partial y_{0m}/\partial DV$ are calculated according to the movement of mesh points with variation of planform shape design variables [Eqs. (23)]. And from Eq. (11)

$$\frac{\partial S_{12}}{\partial DV} = \left[\frac{\partial x_{01}}{\partial DV} - \frac{\partial x_{02}}{\partial DV} - S_{12}\left(\frac{\partial y_{01}}{\partial DV} - \frac{\partial y_{02}}{\partial DV}\right)\right] \Big/ (y_{01} - y_{02}) \tag{A9}$$

$$\frac{\partial S_{34}}{\partial DV} = \left[\frac{\partial x_{03}}{\partial DV} - \frac{\partial x_{04}}{\partial DV} - S_{34}\left(\frac{\partial y_{03}}{\partial DV} - \frac{\partial y_{04}}{\partial DV}\right)\right] \Big/ (y_{03} - y_{04}) \tag{A10}$$

3) $\bar{K}$ is evaluated at $(\bar{x}_0, \bar{y}_0)$, the center of the integrating area of the source element. Thus,

$$\frac{\partial \bar{K}}{\partial DV} = \left(\frac{\partial \bar{K}}{\partial \bar{x}_0}\right)\frac{\partial \bar{x}_0}{\partial DV} + \left(\frac{\partial \bar{K}}{\partial \bar{y}_0}\right)\frac{\partial \bar{y}_0}{\partial DV} \tag{A11}$$

From Eq. (6) the derivatives of the unsteady factor with respect to the centroid coordinates are

$$\frac{\partial \bar{K}}{\partial \bar{x}_0} = \left(\frac{\beta^2 \bar{y}_0^2}{R^2 \bar{x}_0} - i\hat{k}\right)\bar{K} + \frac{M^2 \bar{y}_0^2}{2\bar{x}_0}e^{-i\hat{k}\bar{x}_0} \times \left\{e^{-i\hat{k}\bar{X}_1}\left[\frac{\bar{x}_0 + \bar{X}_1}{M^3(\bar{X}_1^2 + \bar{y}_0^2)^{3/2}} - \frac{\bar{x}_0^2 + \beta^2\bar{X}_1^2}{R^2(\bar{x}_0 + \bar{X}_1)^2} + i\frac{\hat{k}}{MR}\right] + e^{-i\hat{k}\bar{X}_2}\left[\frac{\bar{x}_0 + \bar{X}_2}{M^3(\bar{X}_2^2 + \bar{y}_0^2)^{3/2}} - \frac{\bar{x}_0^2 + \beta^2\bar{X}_1^2}{R^2(\bar{x}_0 + \bar{X}_2)^2} - i\frac{\hat{k}}{MR}\right]\right\} \tag{A12}$$

$$\frac{\partial \bar{K}}{\partial \bar{y}_0} = \frac{2R^2 - \beta^2 \bar{y}_0^2}{\bar{y}_0 R^2}\bar{K} - \frac{M^2 \bar{y}_0^2}{2\bar{x}_0} e^{-i\hat{k}\bar{x}_0} \times \left\{ \frac{3R\bar{y}_0}{M^2} \int_{\bar{X}_1}^{\bar{X}_2} \frac{e^{-i\hat{k}\nu}}{(\bar{y}_0^2 + \nu^2)^{5/2}} \, d\nu + e^{-i\hat{k}\bar{X}_1} \left[\frac{1}{M(\bar{X}_1^2 + \bar{y}_0^2)^{3/2}} - \frac{M^2\bar{x}_0 - 2MR}{R^2(\bar{x}_0 + \bar{X}_1)^2} + i\frac{\hat{k}M}{R(\bar{x}_0 + \bar{X}_1)} \right] + e^{-i\hat{k}\bar{X}_2} \left[\frac{1}{M(\bar{X}_2^2 + \bar{y}_0^2)^{3/2}} - \frac{M^2\bar{x}_0 - 2MR}{R^2(\bar{x}_0 + \bar{X}_2)^2} - i\frac{\hat{k}M}{R(\bar{x}_0 + \bar{X}_1)} \right] \right\} \tag{A13}$$

The case of a panel inducing upwash on itself [Eqs. (22) and (23)] is differentiated in a same manner.

Acknowledgments

This research was supported by NASA Langley Research Center; the Grant Monitor was J.-F. Barthelemy. This paper was also supported by the National Science Foundation. This support is gratefully acknowledged.

References

[1]Sobieszczanski-Sobieski, J., and Chopra, I., "Multidisciplinary Optimization of Aeronautical Systems," *Journal of Aircraft*, Vol. 27, No. 12, 1990, pp. 977, 978.

[2]Schmit, L. A., "Structural Optimization — Some Key Ideas and Insights," *New Directions in Optimum Structural Design*, edited by E. Atrek, R. H. Gallagher, K. M. Ragsdell, and O. C. Zienkiewicz, Wiley, New York, 1984.

[3]Barthelemy, J.-F. M., and Haftka, R. T., "Recent Advances in Approximation Concepts for Optimum Structural Design," NASA TM 104032, March 1991.

[4]Haftka, R. T., and Gurdal, Z., *Elements of Structural Optimization*, 3rd ed., Martinus–Nijhoff, Dordrecht, The Netherlands, 1992.

[5]Becker, J., Weiss, F., and Sensburg, O., "Compatibility Aspects of Active Control Technologies with Aircraft Structural Design," *Structural Control*, edited by H. H. E. Leipholz, Martinus–Nijhoff, Dordrecht, The Netherlands, 1987.

[6]Noll, T., Austin, E., Donely, S., Graham, G., Harris, T., Kaynes, I., Lee, B., and Sparrow, J., "Impact of Active Controls Technology on Structural Integrity," *Journal of Aircraft*, Vol. 30, No. 6, 1993, pp. 985–992.

[7]Noll, T. E., and Eastep, F. E., "Editorial: Active Flexible Wing Program," *Journal of Aircraft*, Vol. 32, No. 1, 1995, p. 9.

[8]Livne, E., Schmit, L. A., and Friedmann, P. P., "Towards an Integrated Approach to the Optimum Design of Actively Controlled Composite Wings," *Journal of Aircraft*, Vol. 27, No. 12, 1990, pp. 979–992.

[9]Livne, E., Schmit, L. A., and Friedmann, P. P., "Exploratory Design Studies Using an Integrated Multidisciplinary Synthesis Capability for Actively Controlled Composite Wings," *AIAA Journal*, Vol. 30, No. 5, 1992, pp. 1171–1179.

[10]Livne, E., Friedmann, P. P., and Schmit, L. A., "Integrated Aeroservoelastic Wing Synthesis by Nonlinear Programming/Approximation Concepts," *Journal of Guidance, Control, and Dynamics*, Vol. 15, No. 4, 1992, pp. 985–993.

[11]Livne, E., "Alternative Approximations for Integrated Control/Structure Aeroservoelastic Synthesis," *AIAA Journal*, Vol. 31, No. 6, 1993, pp. 1100–1108.

[12]Livne, E., and Li, W.-L., "Aeroservoelastic Aspects of Wing/Control Surface Planform Shape Optimization," *AIAA Journal*, Vol. 33, No. 2, 1995, pp. 302–311.

[13]Haftka, R. T., and Yates, C. E., Jr., "On Repetitive Flutter Calculations in Structural Design," *Journal of Aircraft*, Vol. 13, No. 7, 1976, pp. 454–461.

[14]Giunta, A. A., Dudley, J. M., Narducci, R., Grossman, B., Haftka, R. T., Mason, W. H., and Watson, L. T., "Noisy Aerodynamic Response and Smooth Approximations in HSCT Design," *Proceedings of the AIAA/USAF/NASA/ISSMO 5th Symposium on Multidisciplinary Analysis and Optimization* (Panama City, FL), AIAA, Washington, DC, 1994.

[15]Chen, P. C., and Liu, D. D., "Unsteady Supersonic Computations of Arbitrary Wing-Body Configurations Including External Stores," *Journal of Aircraft*, Vol. 27, No. 2, 1990, pp. 108–116.

[16]Chen, P. C., Lee, H. W., and Liu, D. D., "Unsteady Subsonic Aerodynamics for Bodies and Wings with External Stores Including Wake Effect," *Journal of Aircraft*, Vol. 30, No. 5, 1993, pp. 618–628.

[17]Rowe, W. S., "Comparison of Analysis Methods Used in Lifting Surface Theory," *Computational Methods in Potential Aerodynamics*, edited by L. Morino, Springer–Verlag, Berlin, 1986, pp. 197–240.

[18]Yates, C. E., Jr., "Aerodynamic Sensitivities from Subsonic, Sonic, and Supersonic Unsteady, Nonplanar Lifting Surface Theory," NASA TM 100502, Sept. 1987.

[19]Yates, C. E., Jr., "Integral Equation Methods in Steady and Unsteady Subsonic, Transonic and Supersonic Aerodynamics for Interdisciplinary Design," NASA TM 102677, May 1990.

[20]Ueda, T., and Dowell, E. H., "A New Solution Method for Lifting Surfaces in Subsonic Flow," *AIAA Journal*, Vol. 20, No. 3, 1982, pp. 348–355.

[21]Eversman, W., and Pitt, D. M., "Hybrid Doublet Lattice/Doublet Point Method for Lifting Surfaces in Subsonic Flow," *Journal of Aircraft*, Vol. 28, No. 9, 1991, pp. 572–578.

[22]Ueda, T., and Dowell, E. H., "Doublet-Point Method for Supersonic Unsteady Lifting Surfaces," *AIAA Journal*, Vol. 22, No. 2, 1984, pp. 179–186.

[23]Eversman, W., "The Supersonic Doublet Point Method and Its Implementation in a Program for Subsonic and Supersonic Airforces for Oscillating Lifting Surfaces," Dept. of Mechanical and Aerospace Engineering, Univ. of Missouri — Rolla, MO, May 1986.

[24]Roger, K. L., "Airplane Math Modeling Methods for Active Control Design," *Structural Aspects of Active Controls*, CP-228, AGARD, Aug. 1977, pp. 4–11.

[25]Cho, J., and Williams, M. H., "S-Plane Aerodynamics of Nonplanar Lifting Surfaces," *Journal of Aircraft*, Vol. 30, No. 4, 1993, pp. 433–438.

[26]Appa, K., "Constant Pressure Panel Method for Supersonic Unsteady Airload Analysis," *Journal of Aircraft*, Vol. 24, No. 10, 1987, pp. 696–702.

[27]Ueda, T., "Expansion Series of Integral Functions Occurring in Unsteady Aerodynamics," *Journal of Aircraft*, Vol. 19, No. 4, 1982, pp. 345–347.

[28]Livne, E., "Equivalent Plate Structural Modeling for Wing Shape Optimization Including Transverse Shear," *AIAA Journal*, Vol. 32, No. 6, 1994, pp. 1278–1288.

[29]Harvey, M., "Design Oriented Finite Element Structural Modeling for Wing Planform Shape Optimization," M.S. Thesis, Dept. of Aeronautics and Astronautics, Univ. of Washington, Seattle, WA, 1993.

[30]Stark, V. J. E., "On the Approximation of the Normal Velocity on Oscillating Wings," *AIAA Journal*, Vol. 4, No. 12, 1966, pp. 2236–2239.

[31]Van Niekerk, B., "Computation of Second Order Accurate Unsteady Aerodynamic Generalized Forces," *AIAA Journal*, Vol. 24, No. 3, 1986, pp. 492–498.

[32]Golub, G. H., and Van Loan, C. F., *Matrix Computations*, 2nd ed., The Johns Hopkins Univ. Press, Baltimore, MD, 1989.

[33]Woodcock, D. L., "Comparison of Methods Used in Lifting Surface Theory," AGARD 583, Jan. 1971.

[34]Li, W.-L., and Livne, E., "Analytic Sensitivities and Approximations in Supersonic and Subsonic Wing/Control Surface Unsteady Aerodynamics," AIAA Paper 95-1219, April 1995.

[35]Cunningham, A. M., Jr., "Oscillatory Supersonic Kernel Function Method for Interfering Surfaces," *Journal of Aircraft*, Vol. 11, No. 11, 1974, pp. 664–670.

[36]Nissim, E., and Lottati, I., "Supersonic Three Dimensional Oscillatory Piecewise Continuous Kernel Function Method," *Journal of Aircraft*, Vol. 20, No. 8, 1983, pp. 574–681.